Resonant inelastic x-ray scattering at the F 1*s* photoabsorption edge in LiF: Interplay of excitonic and conduction states, and Stokes' doubling

A. Kikas,[1] T. Käämbre,[1] A. Saar,[1] K. Kooser,[1] E. Nõmmiste,[1] I. Martinson,[2] V. Kimberg,[3] S. Polyutov,[3] and F. Gel'mukhanov[3]
[1]*Institute of Physics, University of Tartu, Riia 142, EE-51014 Tartu, Estonia*
[2]*Department of Physics, Lund University, P.O. Box 118, SE-22100 Lund, Sweden*
[3]*Theoretical Chemistry, Roslagstullsbacken 15, Royal Institute of Technology, SE-106 91 Stockholm, Sweden*
(Received 4 December 2003; revised manuscript received 12 April 2004; published 5 August 2004)

The excitation-decay processes at the F 1*s* photoabsorption edge in LiF crystal are studied using resonant inelastic x-ray scattering spectroscopy. The Raman-type linear dispersion and the narrowing of the x-ray fluorescence peak are observed at resonant excitation. A theoretical model based on the Kramers-Heisenberg formula describes well the main features in fluorescence spectra and allows one to separate the contributions of the exciton and the conduction states in the scattering spectra. At the same time, the role of the shape of the spectral distribution within the incident radiation is emphasized as being critically sensitive to the number, kind, and onset of the spectral features which finally appear in the scattering spectra at a particular incident photon energy, particularly in the subthreshold excitation region.

DOI: 10.1103/PhysRevB.70.085102 PACS number(s): 78.70.En, 78.70.Ck, 71.35.−y

I. INTRODUCTION

Traditionally, the x-ray photoabsorption and the following x-ray emission (XE) events were treated as temporally separated processes. Such simplified treatment is nevertheless well known to provide good agreement with the experimental XE spectra when the excitation is well displaced from an absorption resonance. At the same time this approach avoids loading the computation with details related to the excitation. However, that kind of theoretical treatment was unable to reproduce the radiation spectra, which are measured when the energy of the exciting photons is in the vicinity of photoabsorption resonances. In order to avoid such discrepancies the whole (absorption followed by emission) process has then instead been treated as a single event of scattering, theoretically based on the resonant term in the Kramers-Heisenberg formula.[1] The whole process is then known as the resonant inelastic x-ray scattering (RIXS), or resonant x-ray Raman scattering.

Due to the dipole selection rules applicable in the soft x-ray spectral region, and the (tunable) femtosecond duration of the process, information becomes retrievable concerning the symmetry in electronic structure, fast charge transfer, and phonon effects. Therefore, in recent years RIXS has attracted attention as a source capable of providing a unique variety of information about the dynamics of electron excitations[2,3] and the electronic structure of solids.[4–6]

The aim of this paper is to study how the core excitons (electron-core-hole bound states) are reflected in RIXS. For this we present the resonantly excited XE spectra at the F 1*s* photoabsorption edge of LiF. We also performed a simulation, using a model based on resonant scattering theory. Comparison of experimental and simulated spectra allows us to understand the peculiarities of resonant scattering at the photoabsorption threshold.

As an object of study, LiF was primarily considered as a model ionic solid, with the chemical bond containing only negligible contributions of covalent character. Typically, alkali halide photoabsorption spectra contain sharp excitonic peaks, which energetically lie below the broad absorption band. At this point LiF, with the excitonic peaks weak if at all present, does not quite follow a typical pattern. Nevertheless, an earlier study of the fluorine *KLL* resonant Auger spectra indicated that two core excitons are indeed created upon the F 1*s* photoabsorption at threshold.[7] It has also been shown that in the calculations of the F *K* photoabsorption spectrum of LiF, an agreement with the experiment cannot be achieved without taking the electron-core hole interaction into account.[8] Recently, the excitonic effects at the F 1*s* photoabsorption in LiF were even found significant in a nonresonant inelastic hard x-ray scattering study.[9]

In this paper we investigate the evolution of the RIXS spectra under core excitation in the vicinity of the F *K* edge of LiF. Special attention is paid to excitations closely *below* the core photoabsorption threshold. We have found that three qualitatively different mechanisms are responsible for the formation of the fluorescent spectral envelope: (1) The dispersive (truncated) low-energy tail which resembles an inverted photoabsorption profile for large negative detunings and which converges into the narrow nondispersive band of off-resonant emission as the excitation energy approaches the photoabsorption edge; (2) a dispersive low intensity peak resulting from inelastic scattering via an excitonic intermediate state; and (3) the nondispersive contribution which is the result of stray light excitation.

We have found that the effect of anomalously strong enhancement of the stray light contribution to the RIXS spectra occurs when the quasicontinuum part of the photoabsorption dominates over the excitonic resonance. The origin of this enhancement lies in the large spectral width of the stray light contribution, whereby the integral intensity may become non-negligible, although the intensity is low at any particular energy.

The asymmetric low energy tail was observed recently in the RIXS spectra of Cu and Ni metals.[10] Now we see a similar effect in a qualitatively different system, insulator

LiF. Our investigations as well as the results of Ref. 10 show that such unusual structure of the RIXS spectral shape is quite general phenomenon. This means that the study of low energy tails of RIXS spectra provides an alternative technique (in addition to x-ray photoabsorption) to explore the electronic structure of unoccupied states. This fact is of the crucial importance in investigations of not only near edge x-ray absorption fine structure, but even *extended* x-ray absorption fine structure (EXAFS) of disordered systems. Contrary to the conventional EXAFS techniques, EXAFS measured in RIXS mode gives unique opportunity for a complete structure determination of gaseous and amorphous systems. We will explain this in more detail in Sec. III B.

II. EXPERIMENT

The experiments were performed on the "bulk" endstation at beamline I511 at MAX-Lab, Lund, Sweden.[11] The radiation source at this beamline is an undulator which contains 49 periods of 52 mm, with a $K_{\max}=2.7$. The third harmonic of the undulator was used in the experiments. The resolution of the beamline monochromator (a modified version of SX700 by Zeiss) was set to 0.3 eV, and the *c* value of 2.25 was used. The resolution of the grazing incidence, Rowland circle mounted (Nordgren type) XE spectrometer on the endstation was also set to 0.3 eV. The sample was a LiF single crystal, which was cleaved shortly before introducing it into the vacuum system. The base pressure of the system was approximately $1\cdot10^{-9}$ Torr. The experiments were performed at room temperature. The incidence angle of the incoming light was set to 60° with respect to sample surface normal and the XE was measured along the direction of the electric vector of the incident (linearly polarized) radiation.

Figure 1 gives an overview of the measured XE spectra for the excitations in the vicinity of the F 1*s* photoabsorption threshold. The top curve in Fig. 1 displays a fluorescence spectrum at nonresonant excitation (excited at 732 eV photon energy). The fluorine K_α XE peak is seen at 677.8 eV. This peak indicates a transition of an electron from the F 2*p* (valence) states into an F 1*s* core hole. The full width at half maximum of this peak changes significantly at the photoionization threshold, varying from 0.8 eV [spectrum (*d*) excited at 689.8 eV photon energy] to 1.6 eV [spectrum (*e*) with excitation energy 690.8 eV]. Note that for off-resonant excitation [spectrum (*n*)] it has a value of 1.2 eV. Such narrowing at 689.8 eV excitation suggests the creation of a core exciton.[12] In the 681–682 eV energy range, satellite peaks appear, which originate in the XE initial states containing an additional vacancy in the valence band.[13,14] These satellites appear for excitation energies above approximately 720 eV.

It can be seen that the spectra measured at low excitation energies consist of two distinguishable groups of features. One of these groups retains constant emission energy (677.8 eV) which coincides with the F K_α nonresonant XE peak, whereas the other group of features consists mainly of a wide band with a steeper high energy flank which shifts to higher energies together with the excitation energy at approximately constant energy loss. The latter thus behaves in a manner characteristic of the inelastic x-ray (Raman) scattering. At the photoabsorption threshold this structure merges into the K_α characteristic emission line. It should be emphasized that the absence of satellite peaks at 681–682 eV excludes the possibility that the emission in the first group (retaining constant emission energy) could stem from excitation with higher energy photons (from multiple undulator harmonics), which would pass through the monochromator in higher orders of diffraction.

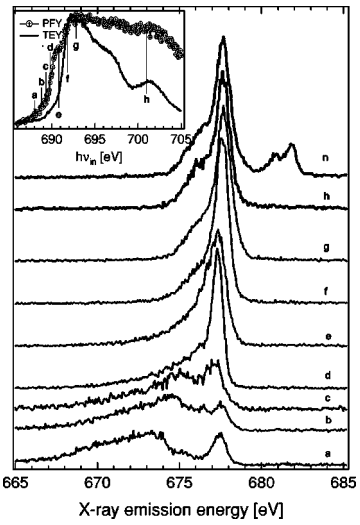

FIG. 1. The scattering spectra recorded at excitation energies (as shown in the inset) in the fluorine 1*s* absorption resonance range. Inset: the F 1*s* photoabsorption spectrum of LiF,[7] measured as the total electron yield (line), compared to the partial fluorescence yield (measured in a 670–680 eV energy window) excitation spectrum (circles). Excitation energies: (a) $\omega=688$ eV, (b) $\omega=688.8$ eV, (c) $\omega=689.3$ eV, (d) $\omega=689.8$ eV, (e) $\omega=690.8$ eV, (f) $\omega=691.8$ eV, (g) $\omega=692.9$ eV, (h) $\omega=701$ eV, (n) $\omega=732$ eV.

Considering the earlier, the presence of two such groups can then be interpreted in the following way: The Raman-like component appears as a result of the excitation of the Lorentzian tail of the photoabsorption resonance. The presence of the K_α fluorescence peak in the subthreshold excited spectra, on the other hand, is due to the excitation of the characteristic K_α fluorescence by photons which originate from the high energy tail of the incident photon spectral distribution. The appearance of this peak in RIXS spectra has become known as Stokes doubling.[15]

III. THEORY

A. Cross section of resonant x-ray Raman scattering

The RIXS process is a one-step coherent process which incorporates the core excitation and the de-excitation with the emission of the final x-ray photon with an energy ω'. The cross section of the resonant scattering of an incident photon with the frequency ω is computed using the Kramers-Heisenberg formula[1,2] (here we use atomic units)

$$\sigma(\omega',\omega)=r_0^2\frac{\omega'}{\omega}\sum_f\int d\omega_1|F_f|^2\Delta[\omega_1-\omega' - (E_f-E_0),\Gamma_f]\Phi(\omega_1-\omega), \quad (1)$$

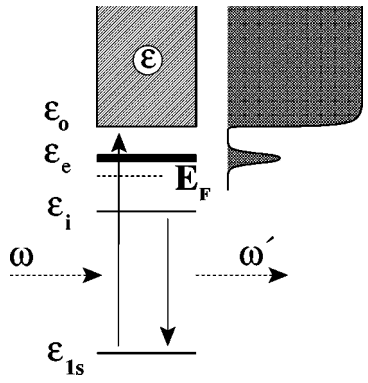

FIG. 2. The scheme of transitions (see text for details). The right-hand side panel shows schematically the photoabsorption profile.

$$F_f = \sum_c \frac{D'_{fc} D_{c0}}{\omega_1 - (E_c - E_0) + \imath\Gamma}.$$

Here $r_0 \approx 2.82 \times 10^{-13}$ cm is the classical electron radius; E_j is the total energy of the electron state j [$j=0$ (ground state), c (core-excited state), f (final state)]; Γ and Γ_f are the lifetime broadenings [half width at half maximum (HWHM)] of the core excited and the final states, respectively; $D_{c0} = (\mathbf{e}\cdot\mathbf{d}_{c0})$, $D'_{fc} = (\mathbf{d}_{fc}\cdot\mathbf{e}')$ are the dipole matrix elements multiplied by the polarization vectors of the incident ($\mathbf{e}$) and the final ($\mathbf{e}'$) photons; $\Delta(\Omega,\Gamma) = \Gamma/\pi(\Omega^2+\Gamma^2)$ where Ω is the detuning frequency. The spectral distribution of the incident radiation $\Phi(\omega_1-\omega)$ takes on a maximum when $\omega_1=\omega$.

For the model shown in Fig. 2 the cross section I reads (see also Ref. 3):

$$\sigma(\omega',\omega) = \sum_i \zeta_i \int_{E_F}^{\infty} d\varepsilon \int d\omega_1 \frac{\rho(\varepsilon)}{(\omega_1 - \omega_{\varepsilon,1s})^2 + \Gamma^2} \times \Delta(\omega_1 - \omega' - \omega_{\varepsilon,i}, \Gamma_f)\Phi(\omega_1 - \omega). \quad (2)$$

Here $\omega_{\varepsilon,i} = \varepsilon - \varepsilon_i$ and $\omega_{\varepsilon,1s} = \varepsilon - \varepsilon_{1s}$; ε is the energy of the conductivity electron, ε_i is the energy of occupied orbital i, ε_{1s} is the energy of the $1s$ electron. All unessential constants are collected in

$$\zeta_i = r_0^2 |D'_{i,1s} D_{1s,e}|^2 \frac{\Gamma\omega'}{\pi\omega}. \quad (3)$$

The density of unoccupied states for the studied model Fig. 2 reads

$$\rho(\varepsilon) = g(\varepsilon - \varepsilon_e, \gamma_e) + c(\varepsilon)\Theta(\varepsilon - \varepsilon_0), \quad (4)$$

where $\Theta(x)$ is the Heavyside step function: $\Theta(x)=1$ when $x \geqslant 0$ and $\Theta(x)=0$ if $x \leqslant 0$. The normalized gaussian

$$g(\varepsilon - \varepsilon_e, \gamma_e) = \frac{1}{\gamma_e}\sqrt{\frac{\ln 2}{\pi}} \exp\left[-\left(\frac{\varepsilon - \varepsilon_e}{\gamma_e}\right)^2 \ln 2 \right] \quad (5)$$

models phonon broadening of the excitonic photoabsorption resonance, $1s \to e$, while the continuum distribution $c(\varepsilon)$ mimics the quasicontinuum part of the photoabsorption (see Fig. 2). The width γ_e describes the vibrational broadening of the excitonic peak. The ratio of squared transition matrix elements $c(\epsilon) = |D_{1s,\varepsilon}/D_{1s,e}|^2$ is related to the ratio ξ of the photoabsorption intensities I of the edge jump and the excitonic peak

$$\xi \equiv \frac{I_{\text{edge jump}}}{I_{\text{exc}}} = \frac{\pi\Gamma c(\varepsilon_0)}{f(\gamma_e/\Gamma)}, \quad (6)$$

$$f(\alpha) = \frac{1}{\alpha}\sqrt{\frac{\ln 2}{\pi}} \int_{+\infty}^{-\infty} \frac{\exp[-(x/\alpha)^2 \ln 2]}{x^2+1} dx.$$

Usually the lifetime broadening of the final state Γ_f is small in comparison with Γ. We therefore neglect Γ_f in the following.

In our model [see Eq. (4)], it is natural to divide the RIXS cross section into the excitonic and the continuum contributions

$$\sigma(\omega',\omega) = \sigma_{\text{exc}}(\omega',\omega) + \sigma_{\text{cont}}(\omega',\omega), \quad (7)$$

where

$$\sigma_{\text{exc}}(\omega',\omega) = \sum_i \frac{\zeta_i \tilde{\Phi}(\omega' - \omega + \omega_{e,i})}{(\omega' - \omega_{i,1s})^2 + \Gamma^2},$$

$$\sigma_{\text{count}}(\omega',\omega) = \sum_i \frac{\zeta_i \int_{\varepsilon_0}^{\infty} c(\varepsilon)\Phi(\omega' - \omega + \omega_{\varepsilon,i}) d\varepsilon}{(\omega' - \omega_{i,1s})^2 + \Gamma^2},$$

$$\tilde{\Phi}(\omega' - \omega + \omega_{e,i}) = \int_{-\infty}^{\infty} g(\varepsilon - \varepsilon_e, \gamma_e)\Phi(\omega' + \varepsilon - \varepsilon_i - \omega) d\varepsilon. \quad (8)$$

B. Scattering of narrow band light beam

It is instructive to understand the structure of the RIXS cross section when the spectral distribution $\Phi(\omega_1-\omega)$ is almost monochromatic: $\Phi(\omega_1-\omega) \approx \Phi_M(\omega_1-\omega)$. We approximate the quasimonochromatic narrow distribution by the normalized gaussian [Eq. (5)] with HWHM γ:

$$\Phi_M(\omega_1 - \omega) = g(\omega_1 - \omega, \gamma). \quad (9)$$

When γ is small as compared to Γ and to the characteristic energy scale of a change of $c(\varepsilon)$ the cross section [Eq. (8)] reads

$$\sigma_{\text{exc}}(\omega',\omega) = \sum_i \zeta_i \frac{g(\omega' - \omega + \omega_{e,i}, \tilde{\gamma})}{(\omega - \omega_{e,1s})^2 + \Gamma^2},$$

$$\tilde{\gamma} = \sqrt{\gamma_e^2 + \gamma^2}, \quad (10)$$

$$\sigma_{\text{cont}}(\omega',\omega) = \sum_i \zeta_i \left[\frac{c(\omega - \omega' + \varepsilon_i)\Theta(\omega - \omega' + \varepsilon_i - \varepsilon_0)}{(\omega' - \omega_{i,1s})^2 + \Gamma^2} \right].$$

One can see two contributions σ_{exc} and σ_{cont} which follow the Raman dispersion law. The "continuum" part σ_{cont} copies

approximately the inverted continuum part of the x-ray absorption spectrum. However, $\sigma_{\rm cont}$ decreases faster than the photoabsorption profile $\sigma(\omega-\omega'+\varepsilon_i)$ due to the Lorentzian $1/[(\omega'-\omega_{i,1s})^2+\Gamma^2]$. It is important to note that $\sigma_{\rm cont}(\omega',\omega)$ has the Raman dispersion behavior only when the excitation energy is tuned below the absorption edge $\omega<\omega_{\varepsilon 0,1s}$. The cross section $\sigma_{\rm cont}(\omega',\omega)$ becomes narrow and copies the Lorentzian $1/[(\omega'-\omega_{i,1s})^2+\Gamma^2]$, when ω crosses the edge $\omega-\omega_{\varepsilon 0,1s}>\Gamma$. This is seen from the identity $\Theta(\omega-\omega'+\varepsilon_i-\varepsilon_0)=\Theta[\omega-\omega_{\varepsilon 0,1s}-(\omega'-\omega_{i,1s})]$. Such behavior of $\sigma_{\rm cont}(\omega',\omega)$ is confirmed by numerical simulations as well as by the experiment (see the discussion of peak C in Sec. IV). So we see that $\sigma_{\rm cont}(\omega',\omega)$ resembles the inverted photoabsorption profile for large negative detunings from the continuum edge and $\sigma_{\rm cont}(\omega',\omega)$ transforms into a Lorentzian when ω exceeds the edge of continuum photoabsorption $\omega_{\varepsilon 0,1s}$ [here the peak position of $\sigma_{\rm cont}(\omega',\omega)$ does not depend on ω].

A comparison with the experimental RIXS profile (Fig. 1) shows that Eq. (10) reconstitutes the inverted photoabsorption. However, it does not describe the nondispesive peak near 678 eV. Let us now to discuss the origin of the nondispersive resonance.

EXAFS measured in RIXS mode

The results of our experiment as well as the measurements[10] point out the strong contribution of the inverted photoabsorption in RIXS. Apparently, the measurements of this contribution in the low energy wing of the RIXS profile allows to map the x-ray absorption fine structure (EXAFS). The EXAFS contribution to $c(\varepsilon)$ (10) reads[16]

$$\sigma^{\rm EXAFS}(\omega',\omega)\propto -\Im m\sum_n \mu_n f_n(\pi)\frac{\exp[2\imath(pR_n+\delta)]}{pR_n^2} \tag{11}$$

with the momentum of the photoelectron $p=\sqrt{2\varepsilon}=\sqrt{2(\omega-\omega'+\varepsilon_i)}$. Here, δ is the central-atom phase shift of the photoelectron wave, $f_n(\pi)$ is the backscattering amplitude of photoelectron by nth atom, $\hat{\mathbf{R}}_n=\mathbf{R}_n/\mathrm{R}_n$. Equation (11) shows that the EXAFS measured in the RIXS mode gives qualitatively different and much richer information on the geometric structure of a system compared to the conventional EXAFS measurement. Indeed, we see the strong dependence of the cross section (11) on the mutual orientations of the polarization vectors $\mathbf{e}$, $\mathbf{e}'$, transition dipole moment of the emission, and internuclear radius vector between core-excited atom an neighboring atom $\mathbf{R}_n$:

$$\mu_n=(\hat{\mathbf{d}}_{fc}\cdot\mathbf{e}')^2(\hat{\mathbf{R}}_n\cdot\mathbf{e})^2 \rightarrow\frac{3}{5}[2-\cos^2\vartheta+(\hat{\mathbf{d}}_{fc}\cdot\hat{\mathbf{R}}_n)^2(3\cos^2\vartheta-1)]. \tag{12}$$

Here ϑ is the angle between polarization vectors of the incident and the emitted x-ray photons. The last expression is valid for randomly oriented systems like amorphous solids, liquids or gases. This expression shows the strong anisotropy of EXAFS measured in RIXS mode, which gives an unique opportunity for a complete structure determination of gaseous or amorphous systems.

Here we would like to point out the qualitative distinction of this discussion from our previous theoretical studies of EXAFS.[16] Only now we see clearly how one can get EXAFS from RIXS. Our experimantal results and measurement in Ref. 10 evidence that the x-ray photoabsortion profile (and, hence, EXAFS) can be measured directly as the low energy part of the RIXS spectrum.

C. Stray light contribution

The spectral distribution of the incident radiation can influence significantly the RIXS profile.[2,15,17,18] The spectral function of the incident radiation is formed by the monochromator and consists of two parts; a narrow Bragg line [Eq. (9)] with peak position ω and a broad stray-light distribution which is caused by the diffuse scattering of the undulator spectral distribution $\Phi_u(\omega_1-\omega_u)$ by the dispersive optical element (the grating).[18] Here ω_u is the peak position of a certain undulator harmonic. Evidently, the spectral distribution after monochromator is proportional to the probability of scattering by monochromator and to the undulator function

$$\Phi(\omega_1-\omega)=[\Phi_M(\omega_1-\omega)+\chi\Phi_{\rm diff}(\omega_1-\omega)]\Phi_u(\omega_1-\omega_u), \tag{13}$$

where χ expresses the strength of the diffuse scattering. The origin of the diffuse scattering is given by $\Phi_{\rm diff}(\omega_1-\omega)$ and depends on the monochromator. It can be thermal diffuse scattering caused by thermal fluctuations of the atomic density in the dispersive element. The surface roughness of the optical element (crystal or grating) also gives rise to the diffuse scattering of the light. For example, the thermal diffuse spectral distribution has a typical[19,20]

$$\Phi_{\rm diff}\propto\frac{1}{q^2},\quad \mathbf{q}=\mathbf{k}'-\mathbf{k}-\mathbf{G} \tag{14}$$

falloff of the diffuse wings, where $\mathbf{q}$ is the change of the wave vector of a photon under scattering; $\mathbf{G}$ is the reciprocal lattice vector.

Equation (14) results in the Lorentzian spectral shape of $\Phi_{\rm diff}(\omega_1-\omega)\propto 1/(\omega_1-\omega)^2$ in the wings under elastic and specular scattering of light by crystal or grating. The diffuse scattering caused by the roughness of the reflecting surface or by the inhomogeneities of the grating structure would also result in a similar law for the diffuse scattering—however, with a different behavior in the wings $\Phi_{\rm diff}\propto 1/q^n$. Here we approximate the diffuse distribution $\Phi_{\rm diff}(\omega_1-\omega)$ by a Lorentzian

$$\Phi_{\rm diff}(\omega_1-\omega)=\frac{\Delta^2}{(\omega_1-\omega)^2+\Delta^2}. \tag{15}$$

We estimated HWHM of the diffuse pedestal for grazing incident angles θ as $\Delta\approx\omega\cdot\delta\beta/\theta$. The angular distribution of the scattered x rays is characterized by the width $\delta\beta$ of diffracted light. We estimate $\delta\beta/\theta\approx 0.03$ making use the results of measurements of Ref. 21. This results in $\Delta\approx 20$ eV.

According to the current experimental conditions (the undulator peak maximum was always tuned to the excitation

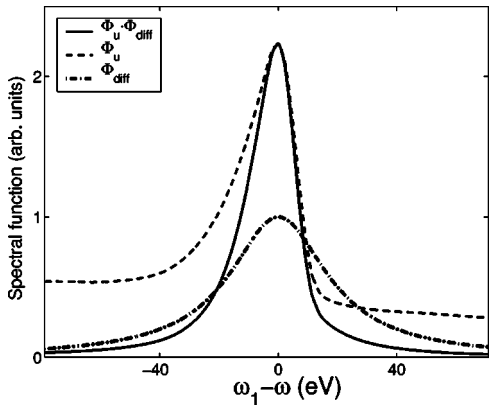

FIG. 3. The spectral functions of the third undulator harmonic Φ_u, the diffuse scattering Φ_{diff}, and stray light $\Phi_S=\Phi_{\text{diff}}\Phi_u$ for $\omega=\omega_u$.

energy) we assume below that $\omega=\omega_u$ and that γ is much smaller than the widths of the undulator and the diffuse distributions. This results in the following representation for the spectral function (13):

$$\Phi(\omega_1-\omega)=\Phi_M(\omega_1-\omega)+\eta\Phi_S(\omega_1-\omega) \tag{16}$$

with a normalized to unit distribution of stray light

$$\Phi_S(\omega_1-\omega_u)=\Phi_{\text{diff}}(\omega_1-\omega)\Phi_u(\omega_1-\omega). \tag{17}$$

The dimensionless parameter $\eta\propto\chi$ is the ratio of the areas of the broad stray light pedestal and narrow monochromatic distribution $\eta=S_S/S_M$. The spectral functions Φ_u, Φ_{diff}, and Φ_S are depicted in Fig. 3.

The experimental data[18] give the following ratio of the peak intensities of the stray light and monochromatic distributions:

$$\frac{\eta\Phi_S^{\max}}{\Phi_M^{\max}}\approx\frac{\eta\gamma}{\gamma_u}\sim 10^{-4}. \tag{18}$$

We get the following estimation:

$$\eta\equiv\frac{S_S}{S_M}\sim 10^{-2} \tag{19}$$

for $\gamma=0.15$ eV and HWHM of the stray light $\gamma_S=20$ eV.

Let us neglect for a while the vibronic broadening of the excitonic state: $\gamma_e=0$. The spectral function [Eq. (16)] says that the RIXS cross section can be divided into the Raman part ($\omega'=\omega-\omega_{e,i}$, or $\omega'=\omega-\omega_{\varepsilon,i}$):

$$\sigma_R\approx\sum_i\frac{\zeta_i}{\Omega^2}[\Phi_M(0)+c(\varepsilon_0)],\quad |\Omega|>\varepsilon_0-\varepsilon_e \tag{20}$$

and a nondispersive ("Stokes") band ($\omega'=\omega_{i,1s}$):

$$\sigma_S\approx\sum_i\frac{\zeta_i}{\Gamma^2}[\Phi_M(-\Omega)+\eta\Phi_u(-\Omega_u)+\sigma(e^{-(\Omega_{\varepsilon_0}/\gamma)^2\ln 2}+\eta)],\quad |\Omega|\gg\gamma,$$

where

$$\Omega=\omega-\omega_{e,i},\quad \Omega_u=\omega_u-\omega_{e,i},\quad \Omega_{\varepsilon_0}=\omega-\omega_{\varepsilon_0,i}. \tag{21}$$

Finally, we get the following estimate for the ratio of the nondispersive and Raman bands for large detunings

$$\frac{\sigma_S}{\sigma_R}\approx\left(\frac{\Omega}{\Gamma}\right)^2\frac{\eta\left(\frac{\gamma}{\gamma_u}+\frac{\gamma}{\pi\Gamma}\xi\right)}{\sqrt{\frac{\ln 2}{\pi}}+\frac{\gamma}{\pi\Gamma}\xi},\quad \left|\frac{\Omega}{\gamma}\right|\gg 1. \tag{22}$$

When the excitonic photoabsorption peak is weak in comparison with the continuum part of photoabsorption, we see strong enhancement of the nondispersive Stokes peak

$$\frac{\sigma_S}{\sigma_R}\approx\left(\frac{\Omega}{\Gamma}\right)^2\eta,\quad \xi\gg 1. \tag{23}$$

For example for $\Omega\approx -2$ eV, $\Gamma=0.15$ eV, and $\eta=10^{-2}$, we get $\sigma_S/\sigma_R\sim 1$. This rough estimation is in a qualitative agreement with the experiment (Fig. 1).

Satellites and the role of higher order radiation

The origin of the nondispersive peak could in principle also lie in excitation by higher undulator harmonics which pass the monochromator in higher orders of diffraction, and from stray light contributions from higher undulator harmonics. The onset of the latter lies at lower energies and therefore these are more intense prior to the monochromator. Because the higher harmonics lie well above the threshold of excitation of satellites, this radiation is capable of creating the satellite structure. On the other hand, the undulator harmonics which lie between the diffraction orders of the monochromator are suppressed due to the rather small characteristic width of the diffuse scattering distribution described earlier: $\Delta\approx 20$ eV [see Eqs. (15) and (17)]. Therefore, it is not unexpected that the experimental spectra (Fig. 1) do not contain any visible trace of the satellites for near threshold excitation $\omega<720$ eV. This indicates that the intensity of the higher order radiation is weak. Thus, the weak higher order radiation can not explain the strong nondispersive peak.

IV. SIMULATIONS

The calculations are based on Eqs. (6), (8), and (15)–(17) with

$$\tilde{\Phi}(\omega'-\omega+\omega_{e,i})\approx g(\omega'-\omega+\omega_{e,i},\tilde{\gamma})+\eta\Phi_S(\omega'-\omega+\omega_{e,i}), \tag{24}$$

where $\tilde{\gamma}$ is defined by Eq. (10). This formula follows directly from the latter part of Eq. (8), because in the experiment $\gamma_e,\gamma\ll\gamma_S$. We assumed in the simulations $c(\varepsilon)=\text{const}$ and used the following input data:

$$\Gamma=0.15\text{ eV};\ \Gamma_f=0;\ \gamma=\gamma_e=0.15\text{ eV},$$

$$\xi=30,\ \eta=0.01,\ \Delta=20\text{ eV},$$

$$\omega_{i,1s}=677.4\text{ eV};\ \omega_{e,1s}=689.75\text{ eV};\ \omega_{\varepsilon_0,1s}=691\text{ eV}. \tag{25}$$

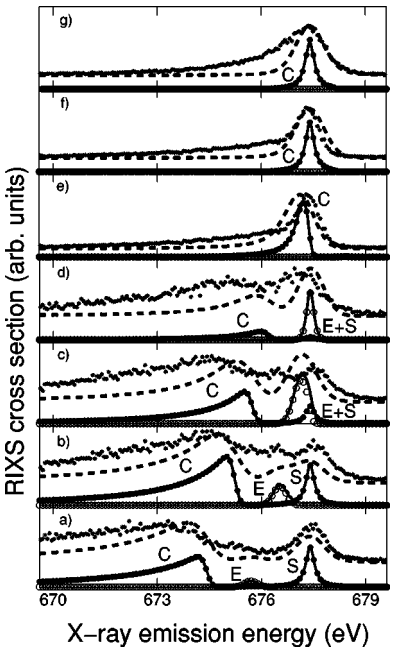

FIG. 4. Calculated RIXS profiles for different excitation energies. The calculated total RIXS profiles are given as solid lines; open and filled circles show the $\sigma_{\mathrm{exc}}(\omega',\omega)$ and the $\sigma_{\mathrm{cont}}(\omega',\omega)$ contributions, respectively; the dashed lines show the total RIXS profile convoluted with a HWHM=0.4 eV gaussian; the experimental results are drawn as stars. The panels (a)–(g) correspond to the same excitation energies as the letters (a)–(g) in Fig. 1.

The results of the simulations are collected in Fig. 4 which shows the fluorescence spectra for different excitation energies. Figure 4(a) shows that the RIXS profile consists of three peaks C, E, and S. The asymmetrical band C is mainly the part of $\sigma_{\mathrm{cont}}(\omega',\omega)$ [Eq. (8)] caused monochromatic light Φ_m [see Eq. (10)]. Both theory and experiment show that band C copies inverted photoabsorption profile for large negative detunings (see discussion in Sec. III B). A similar effect was observed recently for RIXS of Cu and Ni metals.[10] The weak peak E is the contribution from $\sigma_{\mathrm{exc}}(\omega',\omega)$ [Eq. (8)] related only to Φ_m [Eq. (10)]. The origin of peak S is qualitatively different. This peak is related mainly to the continuum part of photoabsorption σ_{cont} and is caused by the stray light $\eta\Phi_S$ [Eq. (16)].

When the excitation energy ω increases [Figs. 4(b)–4(d)] the peaks C and E become stronger and they move to the high energy flank. The intensity of peak E grows faster because here the photon frequency is closer to excitonic peak than to the edge of continuum photoabsorption.

When $\omega=\omega_{e,1s}=689.75$ eV, the positions of peaks E and S coincide [Fig. 4(d)].

Peak E is suppressed strongly for $\omega>\omega_{e,1s}=689.75$ eV because the excitonic level e is not now in resonance with ω [Figs. 4(e)–4(g)]. Now the intensity of the peak C grows fast because ω approaches the continuum edge $\omega_{\varepsilon_0,1s}=691$ eV [Figs. 4(e) and 4(f)]. The intensity of peak C stops to grow when $\omega>\omega_{\varepsilon_0,1s}=691$ eV. Figures 4(e)–4(g) show the narrowing of the peak C to the Lorentzian with HWHM=Γ. This effect was explained at the end of Sec. III B.

The contribution of peak S in the total profile decreases when ω increases because the intensity of this peak almost does not depend on ω, while peaks C and E increase strongly when ω approaches resonant frequencies $\omega_{e,1s}$ and $\omega_{\varepsilon_0,1s}$.

Figure 4 shows that the resonance near $\omega'=677.8$ eV is nondispersive only approximately. Indeed, Figs. 4(c) and 4(e) shows a slight deviation of the peak position from $\omega'=677.8$ eV. The reason for this is that the origin of the peak near $\omega'=677.8$ eV is different for different excitation energies. For large negative detunings it is peak S induced by stray light, while for higher excitation energies it is peak E and C.

The spectral profiles in the simulated spectra are seen to be somewhat narrower than in the experimental data. To some extent the increased width in the experimental spectra can be attributed to phonon broadening in the sample and to the molecular field splitting. Such broadening was mimicked by the convolution of the calculated RIXS profile with a gaussian with HWHM of 0.4 eV (see dashed lines in Fig. 4). The simulation is seen not to reproduce the low energy shoulder in the emission spectra, which has been generally attributed to the covalent character in the cation-fluorine bond,[14] and should therefore be attributed to the valence states with cationic origin. These states are not taken into account in our simulation where the XE final state is treated as a single level.

Because the final state of the XE process is a valence hole, which should mainly originate from the F 2*p* states, the XE spectrum should be similar to the valence band photoelectron spectra. In our experiment, however, (as indicated even in an earlier report, see Ref. 12) the XE spectra are significantly narrower than the corresponding photoelectron spectra.[22] This observation refers to the atomic-like nature of the XE process: A plausible reason for this broadening is that due to the localization of the valence states mainly at the F ion, the XE becomes essentially an intraionic process, which is weakly influenced by the relaxation effects in the vicinity of the core hole site. This suggestion can be supported by the F *KLL* spectra in alkali fluorides,[7] which show the sharp peaks with atomic multiplet structure despite the final state holes being valence holes.

For resonant XE, one might speculate upon the possibility that, at least in part of the absorption events, the coherence between the absorption and emission events can be lost, e.g., due to phonon scattering. In the noncoherent case the resulting emission spectrum should then reflect the (partial) density of the valence states on the core hole site, similarly to the case of nonresonant excitation. Following this trail of thought, one may suggest that the relatively wide nonzero background under the sharp main emission peak can be explained as a result of these noncoherent (absorption and) emission events. (A similar approach has been previously elaborated on carbon and carbon compounds.[4])

However, even in this case the states with F origin are preferred in the XE process due to the partial density of states effects, and thus they should be even more strongly reflected in the coherent part of the emission. However, the mixing between the different states allows transitions from valence states with cationic origin which, however, will take place only after the loss of coherence due to phonon scattering.

Our RIXS spectra indicate the presence of only a single core excitonic state at 689.8 eV excitation energy. This is

similar to the results obtained using nonresonant x-ray scattering,[9] where only one exciton was observed at an energy transfer value of 692.5 eV. From the momentum-transfer dependence and with the help of calculations, it was shown that this exciton has an *s*-type final state. On the other hand, two core excitons were detected by resonant Auger spectroscopy, correspondingly at excitation energies 690.5 and 691.7 eV[7] and it was suggested that these excitons are due to transitions to the final states with the F 3*p* and 4*p* origin.

In the present study, we suggest that the exciton observed at 689.8 eV excitation corresponds to the exciton, which in resonant Auger spectroscopy appears at 690.5 eV excitation, and propose that the minute energy differences emerge from energy-scale calibration issues. This explanation is supported by the similarity of the spectral shapes of the nonresonant inelastic (hard) x-ray scattering in Ref. 9 and the x-ray photoabsorption presented in Ref. 7. A comparable study of photoabsorption of NaF crystal,[24,23] clusters,[25] and molecules[24] supports the idea that the exciton is constituted by transitions to states of *s* symmetry. Although the $s \rightarrow s$ transitions are forbidden in dipole approximation, we believe that the presence of local distortions of the symmetry of higher-lying levels (particularly at surface and near defects) may relax the selection rules to propensity rules, and allow such transitions nevertheless to be seen in the absorption spectra.

The discord with the resonant Auger spectra, which shows a distinguishable pair of excitons can be rationalized if we assume that the higher energy core exciton state in resonant Auger spectroscopy is a result of postcollision interaction (PCI) induced recapture of a slow photoelectron. This mechanism has been previously discussed in the case of Na 1*s* excitations in NaF:[23] right above the 1*s* ionization limit, the outgoing photoelectron can be recaptured into bound state by PCI with a fast Auger electron. As a result, the resonant *KLL* Auger decay spectrum shows a new feature, which is shifted to higher kinetic energies as compared to the normal Auger peak.[7,23] Because such interaction is not observable in the case of radiative decay we indeed do not observe it in RIXS, and on the other hand it also explains why the second exciton was either not seen in the nonresonant x-ray inelastic scattering spectra of LiF.[9]

V. CONCLUSIONS

We propose that the higher energy excitonic state as seen in resonant Auger spectroscopy is a PCI resonance, by comparing our RIXS and the earlier resonant Auger spectroscopy[7,23] as well as the nonresonant x-ray inelastic scattering spectra of LiF.[9]

When comparing the experimental data with the results of the simulations, we find that the RIXS profile consists of three gross features when the excitation energy is tuned far below the photoabsorption edge: first, a broad asymmetric band resembling the photoabsorption spectrum and a small excitonic peak; both follow to the Raman dispersion. The third component arises when the excitation energy is tuned far below the absorption edge: then the high energy peak is caused by the stray light and its position as well as intensity does not depend on the excitation energy. The position of this peak coincides with the frequency of off-resonant emission.

When the excitation energy approaches the photoabsoprtion edge, two dispersive peaks are enhanced strongly. The second peak intensity drops when the excitation energy crosses the excitonic photoabsorption resonance.

When the excitation energy crosses the edge of continuum photoabsorption, the broad asymmetric band dominates and develops into a symmetric Lorentzian. The RIXS spectrum is then formed only by this symmetric Lorentzian, the position of which stops to depend on the excitation energy and coincides with the line of off-resonant emission. Thus, we see clearly that the origin of the nondispersive high energy peak is different for large negative detuning and for excitation near the photoabsorption edge.

Apart from the description of electronic structure and dynamics, our results call attention to two features of RIXS. For the first, RIXS gives a possibility to investigate the nature of photoabsorption in insulators, in which case the resonant Auger spectroscopy is not usable due to charging effects in monocrystals and in the absence of thin samples with sufficiently high quality. For the second, our study shows that RIXS can effectively be used as a tool to estimate details (e.g., intensities at tails) of the photon energy distributions of beamline monochromators.

Furthermore, for the RIXS profiles obtained for excitations sufficiently far below the photoabsorption threshold, the theory holds that EXAFS oscillations should become observable experimentally. Although the intensity of such signal is weak using available light sources, the extra cost of time doing such measurements may well be balanced off by the additional polarization dependence which contains information not accessible by the conventional EXAFS method.

ACKNOWLEDGMENTS

Financial support by the Estonian Science Foundation, the Crafoord Foundation, the Royal Physiographic Society of Lund and EC Programs "Center of Excellence" and "Access to Research Infrastructure" is gratefully acknowledged. The authors also wish to thank staff of the MAX-Lab for the support during measurements. V.K., S.P., and F.G. acknowledge support from the Swedish National Research council (NFR).

[1] T. Åberg and B. Crasemann, in *Resonant Anomalous X-Ray Scattering*, edited by G. Materlik, C. J. Sparks, and K. Fischer (North-Holland, Amsterdam, 1994), p. 430.
[2] F. Gel'mukhanov and H. Ågren, Phys. Rep. **312**, 87 (1999).
[3] J.-E. Rubensson, J. Electron Spectrosc. Relat. Phenom. **110-111**, 135 (2000).
[4] J. A. Carlisle, E. L. Shirley, E. A. Hudson, L. J. Terminello, T. A. Callcott, J. J. Jia, D. L. Ederer, R. C. C. Perera, and F. J. Himpsel, Phys. Rev. Lett. **74**, 1234 (1995).
[5] S. M. Butorin, J. Electron Spectrosc. Relat. Phenom. **110-111**, 213 (2000).
[6] M. Taguchi, L. Braicovich, G. Ghiringhelli, A. Tagliaferri, F. Borgatti, C. Dallera, K. Giarda, and N. B. Brookes, Phys. Rev. B **63**, 235113 (2001).
[7] H. Aksela, E. Kukk, S. Aksela, A. Kikas, E. Nõmmiste, A. Ausmees, and M. Elango, Phys. Rev. B **49**, 3116 (1994).
[8] J. A. Soininen and E. L. Shirley, Phys. Rev. B **64**, 165112 (2001).
[9] K. Hämäläinen, S. Galambosi, J. A. Soininen, E. L. Shirley, J.-P. Rueff, and A. Shukla, Phys. Rev. B **65**, 155111 (2002).
[10] M. Magnuson, J.-E. Rubensson, A. Föhlisch, N. Wassdahl, A. Nilsson, and N. Mårtensson, Phys. Rev. B **68**, 045119 (2003).
[11] R. Denecke, P. Väterlein, M. Bässler, N. Wassdahl, S. Butorin, A. Nilsson, J.-E. Rubensson, J. Nordgren, N. Mårtensson, and R. Nyholm, J. Electron Spectrosc. Relat. Phenom. **103**, 971 (1999).
[12] J.-E. Rubensson, S. Eisebitt, M. Nicodemus, T. Böske, and W. Eberhardt, Phys. Rev. B **50**, 9035 (1994).
[13] M. Oura, T. Mukoyama, M. Taguchi, T. Takeuchi, T. Haruna, and S. Shin, Phys. Rev. Lett. **90**, 173002 (2003).
[14] R. Hessabi and D. S. Urch, J. Chem. Soc., Faraday Trans. **86**, 247 (1990).
[15] F. Gel'mukhanov and H. Ågren, Phys. Rev. A **49**, 4378 (1994); Phys. Lett. A **193**, 375 (1994).
[16] F. Gel'mukhanov and H. Ågren, Phys. Rev. B **50**, 11 121 (1994); F. Gel'mukhanov, O. Plashkevych, and H. Ågren, J. Phys. B **34**, 869 (2001).
[17] S. Aksela, E. Kukk, H. Aksela, and S. Svensson, Phys. Rev. Lett. **74**, 2917 (1995).
[18] R. Feifel, A. Baev, F. Gel'mukhanov, H. Ågren, M. Andersson, G. Öhrwall, M. N. Piancastelli, C. Miron, S. L. Sorensen, A. Naves de Brito, O. Björneholm, L. Karlsson, and S. Svensson, J. Electron Spectrosc. Relat. Phenom. **134**, 49 (2004).
[19] L. D. Landau and E. M. Lifshits, *Electrodynamics of Continuous Media* (Addison-Wesley, Reading, MA, 1984).
[20] E. Weidner, J.-L. Lei, F. Frey, R. Wang, and B. Grushko, J. Alloys Compd. **342**, 156 (2002).
[21] V. A. Chernov, V. I. Kondratiev, N. V. Kovalenko, and S. V. Mytnichenko, Nucl. Instrum. Methods Phys. Res. A **470**, 145 (2001).
[22] F. J. Himpsel, L. J. Terminello, D. A. Lapiano-Smith, E. A. Eklund, and J. J. Barton, Phys. Rev. Lett. **68**, 3611 (1992).
[23] A. Kikas, E. Nõmmiste, R. Ruus, A. Saar, and I. Martinson, Phys. Rev. B **64**, 235120 (2001).
[24] C. M. Teodorescu, A. El Afif, J. M. Esteva, and R. C. Karnatak, Phys. Rev. B **63**, 233106 (2001).
[25] C. M. Teodorescu, J. M. Esteva, M. Womes, A. El Afif, R. C. Karnatak, A. M. Flank, and P. Lagrade, J. Electron Spectrosc. Relat. Phenom. **106**, 233 (2000).